Approximating Optimal State Estimation

Brian F. Farrell and Petros J. Ioannou

Harvard University
Cambridge MA 02138, U.S.A
farrell@deas.harvard.edu, pji@cc.uoa.gr

ABSTRACT

Minimizing forecast error requires accurately specifying the initial state from which the forecast is made by optimally using available observing resources to obtain the most accurate possible analysis. The Kalman filter accomplishes this for linear systems and experience shows that the extended Kalman filter also performs well in nonlinear systems. Unfortunately, the Kalman filter and the extended Kalman filter require computation of the time dependent error covariance matrix which presents a daunting computational burden. However, the dynamically relevant dimension of the forecast error system is generally far smaller than the full state dimension of the forecast model which suggests the use of reduced order error models to obtain near optimal state estimators. A method is described and illustrated for implementing a Kalman filter on a reduced order approximation of the forecast error system. This reduced order system is obtained by balanced truncation of the Hankel operator representation of the full error system. As an example application a reduced order Kalman filter is constructed for a time-dependent quasi-geostrophic storm track model. The accuracy of the state identification by the reduced order Kalman filter is assessed and comparison made to the state estimate obtained by the full Kalman filter and to the estimate obtained using an approximation to 4D-Var. The accuracy assessment is facilitated by formulating the state estimation methods as observer systems. A practical approximation to the reduced order Kalman filter that utilizes 4D-Var algorithms is examined.

1 Introduction

An important component of forecast error is error in the analysis of the initial state from which the forecast is made. Analysis error can be reduced by taking more observations, by taking more accurate observations, by taking observations at locations chosen to better constrain the forecast, and by extracting more information from the observations that are available. The last of these, obtaining the maximum amount of information from observations, is attractive because it makes existing observations more valuable and because, at least for linear systems, there is a solution to the problem of extracting the maximum information from a given set of observations: under appropriate assumptions the problem of extracting the maximum amount of information from a set of observations of a linear system in order to minimize the uncertainty in the state estimate is solved by the Kalman filter (KF) (Kalman, 1960; Ghil and Malanotte-Rizzoli, 1991; Wunch, 1996; Ide et al, 1997; Lermusiaux and Robinson, 1999). Moreover, application of the Kalman filter to the local tangent error equations of a nonlinear system provides a first order approximation to the optimal data assimilation method which is valid in the limit of sufficiently small errors. This nonlinear extension of the KF is referred to as the extended Kalman filter (EKF) (Ghil et al, 1981; Miller et al, 1994; Ide & Ghil, 1997, Ghil, 1997).

Unfortunately, the Kalman filter and the extended Kalman filter require statistical description of the forecast error in the form of the error covariance and obtaining the required error covariance involves integrating a system with dimension equal to the square of the dimension of the forecast system. Direct integration of a system of such high dimension is not feasible. Attempts to circumvent this difficulty (see review of Ghil, 1997) have involved various approximations to the error covariance (Bishop et al, 2001; Tippett et al, 2000) and approximate integration methods (Evensen, 1994; Dee,1995; Fukumori and Malanotte-Rizzoli, 1995;

Cohn and Todling, 1996; Verlaan and Heemink, 1997; Houtekamer and Mitchell, 1998; Hamill, 2005; Kalnay et al 2005).

While the formal dimension of the forecast error system obtained by linearizing the forecast model about a base trajectory is the same as that of the forecast system itself, there are reasons to believe that the effective dimension is far lower. The trajectory of the system state in a high dimensional dynamical system typically lies on a small dimensional subspace of the entire phase space. In chaotic systems all initial conditions approach this attractor which can be embedded in a space of dimension at most $2d+1$, where d is the attractor dimension (Takens, 1981). An estimate of the attractor dimension can be made from the number of positive Lyapunov exponents (the Kaplan-Yorke dimension; Kaplan & Yorke, 1979) but anyway the attractor dimension is bounded above by the number of Lyapunov exponents associated with positive volume growth along the system trajectory in phase space (Illyashenko, 1983). While this is useful conceptually for bounding the dimension of the embedding space, identifying the subspace itself is more difficult in the case of nonlinear and time dependent systems. However, in the case of stochastically forced linear normal systems the analogous subspace to which the solution is primarily confined can be easily found by eigenanalysis of the covariance matrix of the system forced white in space and time. The resulting EOF spectrum typically falls off rapidly in physical models. The eigenvectors may be identified with the modes of the normal operator and the corresponding eigenvalues are the variance accounted for by the modes (North, 1984; Farrell and Ioannou, 1996, (henceforth FI96)). The fact that a restricted number of EOF's account for nearly all of the variance in normal systems shows that the effective dynamical dimension of these systems is small compared with the dimension of their phase space. This notion of quantifying the effective dimension of normal linear systems can be extended to bound the effective dimension of non-normal systems (Farrell and Ioannou, 2001a (henceforth FI01)).

In the case of the tangent linear forecast error system the spectrum of optimal perturbations of the error propagator over the forecast interval typically comprises a few hundred growing structures (Buizza and Palmer, 1995) and Lyapunov spectra for error growth have shown similar numbers of positive exponents (Palmer et al, 1998) which suggests from the above considerations that the effective dimension of the error system for scales resolved by forecast models is $O(10^3)$.

The problem of reducing the order of a linear dynamical system can be cast mathematically as that of finding a finite dimensional representation of the dynamical system so that the Eckart-Schmidt-Mirsky (ESM) theorem (Stewart and Sun, 1990) can be applied to obtain an approximate truncated system with quantifiable error. The ESM theorem states that the optimal k order truncation of an n dimensional matrix in the euclidean or Frobenius norm is the matrix formed by truncating the singular value decomposition of the matrix to its first k singular vectors and singular values. A method for exploiting the ESM theorem to obtain a reduced order approximation to a dynamical system was developed in the context of controlling lumped parameter engineering systems and is called balanced truncation (Moore, 1981; Glover, 1984; Zhou and Doyle, 1998). Balanced truncation was applied to the set of ordinary differential equations approximating the partial differential equations governing perturbation growth in time independent atmospheric flows by FI01.

We first review the method of balanced truncation and then illustrate it with a simple matrix example. Then we apply it to a storm track model (cf Farrell and Ioannou, 2001b). We then review some salient aspects of optimal state estimation using analysis based on an observer model of the assimilation system and discuss the structure of the gain matrix in the presence of model error and the asymptotic behavior of the assimilation error as the number of observations increases. We finally construct a reduced order Kalman filter based on balanced truncation and apply it to a time dependent Lyapunov unstable quasi-geostrophic model of a forecast tangent linear error system with which we examine the approach of an approximation to the optimal observer based on 4D-Var.

2 The storm track model

Consider an idealized model of the midlatitude storm track consisting of a Boussinesq atmosphere with constant stratification and constant shear in thermal wind balance on a β-plane channel with periodic boundary conditions in the zonal, x, direction; solid walls located at two latitudes in the meridional, y, direction and a solid lid at height $z = H$, simulating the tropopause. The observed zonal localization of a midlatitude storm track is simulated in the model by terminating the channel with a linear damping modelling the storm track exit region. The stability properties of such a storm track model are discussed in FI96.

Zonal and meridional lengths are nondimensionalized by $L = 1200\ km$; vertical scales by $H = fL/N = 10\ km$; velocity by $U_0 = 50\ m/s$; and time by $T = L/U_0$, so that a time unit is approximately $6.7\ h$. The Brunt-Vaisala frequency is $N = 10^{-2}\ s^{-1}$, and the Coriolis parameter is $f = 10^{-4}\ s^{-1}$. The corresponding non-dimensional value of the planetary vorticity gradient is $\beta = 0.46$.

The non-dimensional linearized equation which governs evolution of streamfunction perturbations is:

$$\frac{\partial \nabla^2 \psi}{\partial t} \;=\; -\,U(z)\,\nabla^2 D\psi \;-\; \left(\beta \;-\; \frac{d^2U(z)}{dz^2}\right) D\psi \;-\; r(x)\,\nabla^2\psi \quad , \tag{1}$$

in which the perturbation is assumed to be in the form $\psi(x,z,t)\,e^{ily}$, where l is the meridional wavenumber; $\nabla^2\psi$ is the perturbation potential vorticity, with $\nabla^2 \equiv \partial^2/\partial x^2 + \partial^2/\partial z^2 - l^2$; and $D \equiv \partial/\partial x$. The perturbation potential vorticity damping rate $r(x)$ is taken to vary smoothly in the zonal direction with form:

$$r(x) = \frac{\mu}{2}\,\left[2 - \tanh\left(\frac{x-\pi/4}{\delta}\right) \;+\; \tanh\left(\frac{x-7\pi/2}{\delta}\right)\right], \tag{2}$$

in which parameters controlling the maximum damping rate and the width of the damping region have been chosen to be $\mu = 5$ and $\delta = 1.5$, respectively. The mean velocity profile is $U(z) = 0.2 + z$. The zonal extent of the re-entrant channel is $0 < x < 4\pi$; latitudinal walls are located at $y = 0$ and $y = 1$, and the ground and tropopause boundaries are located at $z = 0$ and $z = 1$, respectively. In the following we consider perturbations with $l = 1$. A cross section of the idealized storm track at a given latitude is shown in Fig 1. Conservation of potential temperature at the ground and tropopause provides the boundary conditions:

$$\frac{\partial^2 \psi}{\partial t \partial z} \;=\; -\,U(0)\,D\,\frac{\partial \psi}{\partial z} \;+\; U'(0)\,D\,\psi \;-\; r(x)\,\frac{\partial \psi}{\partial z} \;-\; \Gamma_g\,(D^2 - l^2)\psi \quad \text{at } z \;=\; 0 \quad , \tag{3}$$

$$\frac{\partial^2 \phi}{\partial t \partial z} \;=\; -\,U(1)\,D\,\frac{\partial \psi}{\partial z} \;+\; U'(1)\,D\,\psi \;-\; r(x)\,\frac{\partial \psi}{\partial z} \quad \text{at } z \;=\; 1\,, \tag{4}$$

where $U'(0)$ and $U'(1)$ denote the velocity shear at $z = 0$ and $z = 1$ respectively. The coefficient of Ekman damping $\Gamma_g \;\equiv\; \frac{N}{U_0}\sqrt{\frac{\nu}{2f}}$ is given the value $\Gamma_g \;=\; 0.0632$ corresponding to a vertical eddy momentum diffusion coefficient $\nu = 20\ m^2/s$ in the boundary layer .

The waves evolve with nearly zero damping in the middle third of the channel (a length of $2\pi L \approx 7500$ Km) which models the core of the storm track. Because in this model absolute instabilities do not exist with everywhere westerly flow, the storm track is asymptotically stable for all meridional wavenumbers because all perturbations are eventually absorbed on entering the highly dissipative sponge (FI96).

Two scenarios are investigated. In the first a transiently growing disturbance excited near the western boundary of the storm track is modelled using the reduced order system, the purpose being to illustrate the accuracy of the reduced order model approximation of the autonomous dynamics. In the second, time dependence is added to produce a Lyapunov unstable model of a tangent linear forecast error system, the time mean operator remaining stable, with the purpose of evaluating the accuracy of the Kalman filter obtained by the reduced order model in

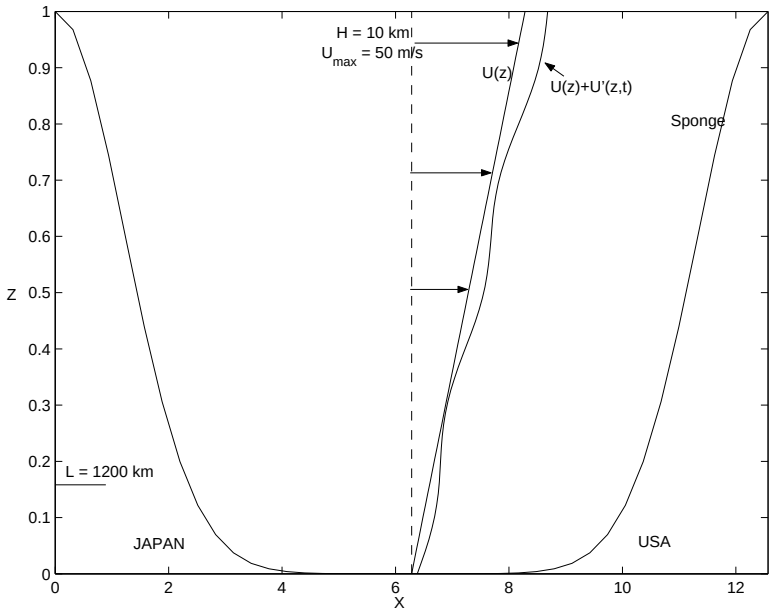

Figure 1: The cross section of the storm tack. Also shown are the sponge layers.

an unstable time dependent system. Such an unstable time dependent system provides an even more stringent test of the state estimator than does the time independent stable and unstable model error systems studied by Todling & Ghil (1994), Ghil & Todling (1996) and Cohn and Todling (1996).

The perturbation dynamics of the time mean storm track are governed by:

$$\frac{d\psi}{dt} = \mathbf{A}\psi \,, \tag{5}$$

where:

$$\mathbf{A} = \left(\nabla^2\right)^{-1} \left(-(0.2+z)\, D\, \nabla^2 - \beta\, D - r(x)\, \nabla^2\right) \,, \tag{6}$$

in which the Helmholtz operator, ∇^2, has been made invertible by incorporating the boundary conditions[1].

The dynamical operator is approximated spectrally in the zonal direction and with finite differences in the vertical. With 40 zonal harmonics and 10 levels in the vertical the resulting dynamical system has $N = 400$ degrees of freedom.

3 Reducing the model order by balanced truncation

Although this storm track model is of small enough dimension for direct numerical solution, we are interested in using it to explore the accuracy of approximate solutions obtained using reduced order models that could be implemented in far larger systems such as arise in numerical forecast.

Before proceeding with the order reduction we must first choose the norm that will be used to measure the accuracy of the approximation. The accuracy is measured by the norm of the euclidean length of the errors incurred in a chosen variable. This norm is the square root of the euclidean inner product in this variable. If another norm is selected to measure the accuracy of the approximation then the most direct method of accounting

[1]For waves with a constant meridional wavenumber l, the operator ∇^2 is invertible even for homogeneous boundary conditions.

for this choice is to transform the variable used to represent the state of the system so that the euclidean inner product in the transformed variable corresponds to the new norm. The reduced order approximate system resulting from balanced transformation will in general depend on the norm chosen. As discussed in FI01, optimal order reduction of dissipative stable normal systems is immediate: it is Galerkin projection of the dynamics onto the least damped modes. Difficulties in the reduction process arise when the system is non-normal in the variable corresponding to the chosen norm. Then Galerkin projection on the least damped modes is suboptimal and the reduction must proceed by including in the retained subspace the distinct subspaces of the preferred excitations and preferred responses of the system. Throughout this paper we have chosen streamfunction as the error variable, the rms of which is to be minimized in the construction of the model order reduction. However, we find that the results do not change qualitatively if the energy norm is chosen instead.

The preferred structures of response of a general non-normal system are revealed by stochastically forcing the system with spatially and temporally uncorrelated unitary forcing and calculating the eigenfunctions of the resulting mean covariance matrix $\mathbf{P} =< \psi\psi^\dagger >$ (the brackets denote an ensemble average, and † the hermitian transpose of a vector or a matrix). The covariance matrix under such forcing is given by:

$$\mathbf{P} \;=\; \int_0^\infty e^{\mathbf{A}t}\, e^{\mathbf{A}^\dagger t}\, dt \;, \tag{7}$$

and this integral is readily calculated by solving the Lyapunov equation (FI96):

$$\mathbf{A}\,\mathbf{P} \;+\; \mathbf{P}\,\mathbf{A}^\dagger \;=-\,\mathbf{I}\;, \tag{8}$$

which $\mathbf{P}$ satisfies, as can be easily verified. The hermitian and positive definite matrix $\mathbf{P}$ characterizes the response of the system and its orthogonal eigenvectors, ordered in decreasing magnitude of their eigenvalue, are the empirical orthogonal functions (EOF's) of the system under spatially and temporally uncorrelated forcing.

In control literature the covariance matrix $\mathbf{P}$ is called the controllability gramian and is given an alternative interpretation as a measure of the efficiency by which forcings place the system in a given state. This alternative deterministic interpretation of the covariance is very useful in predictability and stems from the observation that if we force the system

$$\frac{d\psi}{dt} = \mathbf{A}\psi + \mathbf{f}(t)\;, \tag{9}$$

from $t=-\infty$ to $t=0$, with initial condition $\psi(-\infty)=0$ then all the states that can appear at $t=0$ with square integrable forcings satisfying

$$\int_{-\infty}^{0} \mathbf{f}^\dagger \mathbf{f} dt \le 1\;, \tag{10}$$

are exactly

$$\mathbf{P}^{1/2}\psi \tag{11}$$

with $||\psi|| \le 1$ (for a proof see Dullerud & Paganini (2000) or Farrell & Ioannou (2005)). For example, let $\mathbf{v}_i$ the eigenfunctions of $\mathbf{P}$ with eigenvalues λ_i ordered in descending order in their magnitude, that is $\lambda_1 > \lambda_2 > \cdots$. Then the top eigenfunction $\mathbf{v}_1$, in which as we have see most of the response of the system is concentrated, is also the state that can be most easily forced in the sense that given forcings of unit amplitude then the largest state that can result at $t=0$ is $\sqrt{\lambda_1}\mathbf{v}_1$. In this way the eigenfunctions of the covariance matrix split the state space into an orthonormal basis that identifies the likelihood of occurrence of a given state. This is the reason that in predictability studies in which the impact of uncertain initial conditions is investigated, the initial states are conditioned by the covariance or Mahalanobis metric(Palmer et al, 1998):

$$||\psi||_M^2 \equiv \psi^\dagger \mathbf{P}^{-1}\psi\;. \tag{12}$$

A geometric interpretation of these states is offered by the controllability ellipsoid

$$\psi^\dagger \mathbf{P}^{-1} \psi = 1 \tag{13}$$

which has semimajor axes in the directions of $\mathbf{v}_i$ with length $\sqrt{\lambda_i}$.

The preferred structures of excitation of the system are determined from the stochastic optimal matrix:

$$\mathbf{Q} \;=\; \int_0^\infty e^{\mathbf{A}^\dagger t}\, e^{\mathbf{A}t}\, dt \;\;, \tag{14}$$

the orthogonal eigenvectors of which when ordered in decreasing magnitude of their eigenvalue rank the forcing structures according to their effectiveness in producing the statistically maintained variance (for a deterministic interpretation of $\mathbf{Q}$ see FI01). The eigenvectors of $\mathbf{Q}$ are called the stochastic optimals (SO's) and because of the non-normality of the system are distinct from the EOF's. The stochastic optimal matrix $\mathbf{Q}$ satisfies the back Lyapunov equation:

$$\mathbf{A}^\dagger\, \mathbf{Q} \;+\; \mathbf{Q}\, \mathbf{A} \;=\; -\,\mathbf{I} \;\;. \tag{15}$$

The stochastic optimal matrix $\mathbf{Q}$ is called the observability gramian in control literature and is a given an alternative deterministic interpretation. Let the system

$$\frac{d\psi}{dt} = \mathbf{A}\psi \;, \tag{16}$$

$t = 0$ be at state ψ_0. The states of the system

$$\psi(t) = e^{\mathbf{A}t}\psi_0 \;, \tag{17}$$

produced by this initial condition have square integral norm:

$$\int_0^\infty \psi^\dagger(t)\psi(t)dt = \psi_0^\dagger \mathbf{Q} \psi_0 \;. \tag{18}$$

The eigenvectors of $\mathbf{Q}$, $\mathbf{u}_i$ when ordered in decreasing magnitude of their eigenvalue, μ_i rank the initial conditions in effectiveness in producing square integrable output, and the observability ellipsoid

$$\psi^\dagger \mathbf{Q}^{-1} \psi = 1 \tag{19}$$

which has semimajor axes in the directions of $\mathbf{u}_i$ with length $\sqrt{\mu_i}$, identifies the initial conditions that produce maximum square integrable output, or equivalently, orders the initial states in the degree that they can be identified from observations of the system $\psi(t)$.

Lyapunov equations (8) and (15) have unique positive definite solutions $\mathbf{P}$ and $\mathbf{Q}$ if $\mathbf{A}$ is stable. If the operator $\mathbf{A}$ is not stable, $\mathbf{P}$ and $\mathbf{Q}$ can be obtained by stabilizing the operator by adding Rayleigh friction. Alternatively, finite time horizon $\mathbf{P}$ and $\mathbf{Q}$ matrices can be used to obtain a reduced order system that best approximates the dynamics over a finite time interval. In any case the covariance matrix $\mathbf{P}$ and stochastic optimal matrix $\mathbf{Q}$ or an approximation to these matrices need to be determined or approximated in order to proceed with order reduction by balanced truncation.

For general non-normal systems the observability and controllability ellipsoids are distinct. A successful order reduction must accurately approximate the dynamics by including in the truncation both the directions of the system's response (the dominant eigenfunctions of $\mathbf{P}$) but also the directions in which when the system is forced, it most effectively responds (the dominant eigenfunctions of $\mathbf{Q}$). The fact that the observability and the controllability ellipsoid are distinct is an indication that the directions of greatest response of the system are different from the directions in which it is most effectively forced. If we can identify a coordinate

transformation in which the controllability and observability ellipsoids are the same, then in these balanced coordinates, reduction of the order of the system can proceed by retaining the dominant directions of the common ellipsoid. The semi-major axes of this common ellipsoid in the balanced representation are the Hankel singular vectors and the lengths of the semi-major axes are the Hankel singular values which turn out to be the square root of the eigenvalues of the product of the covariance and stochastic matrix, **PQ**. The balanced truncation thus transforms the internal coordinates of the system so that the transformed covariance matrix **P** and stochastic optimal matrix **Q** become identical and diagonal (while preserving the inner product of the physical variables). The dynamical system is then truncated in these transformed balanced coordinates. The balanced truncation retains a leading subset of empirical orthogonal functions (EOF's) and stochastic optimals (SO) of the dynamical system and preserves the norm. Balanced truncation preserves the stability of the full system and provides an approximation with known error bounds which is found in practice to be nearly optimal (Moore, 1981; Glover, 1984; FI01) as will now be shown.

A successful order reduction must accurately approximate the dynamics of the system which can be expressed as the mapping of all past (square integrable) forcings to all future responses. This linear mapping of inputs to outputs is called the Hankel operator. Application of the ESM theorem to the Hankel operator provides the optimal low order truncation of the dynamics. Remarkably, because of the separation between past forcings and future responses in the Hankel operator representation of the dynamics this operator has finite rank equal to the order of the system; and its singular values, denoted by h, turn out to be the lengths of the semi-major axes of the balanced controllability-observability ellipsoid.

The procedure used to implement balanced truncation is now briefly reviewed. Consider a general k order truncation of the N dimensional system (5):

$$\frac{d\tilde{\psi}_k}{dt} = \mathbf{A}_k \tilde{\psi}_k \,, \tag{20}$$

where $\mathbf{A}_k$ is the reduced $k \times k$ dynamical matrix, with $k < N$, and $\tilde{\psi}_k$ the associated reduced order k-dimensional state vector which is related to the full state vector by the transformation $\tilde{\psi} = \mathbf{X}\tilde{\psi}_k$. Similarly, the reduced state vector $\tilde{\psi}_k$ is related to the full state vector by: $\tilde{\psi}_k = \mathbf{Y}^\dagger \tilde{\psi}$ (the dagger denotes the hermitian transpose of a matrix), which implies that $\mathbf{Y}^\dagger \mathbf{X} = \mathbf{I}_k$, where $\mathbf{I}_k$ is the k-order identity matrix. Matrices $\mathbf{Y}$ and $\mathbf{X}$ determine the transformation from the full system to the reduced system. The matrix $\mathbf{A}_k$, governing the dynamics in (20), is:

$$\mathbf{A}_k = \mathbf{Y}^\dagger \, \mathbf{A} \, \mathbf{X} \,. \tag{21}$$

Details of the construction on the biorthogonal matrices $\mathbf{X}$ and $\mathbf{Y}$ are given in Farrell & Ioannou (2001b).

A measure of the accuracy of the truncation is the maximum difference that can occur between the full system response, $\psi(t)$, and the reduced order system response, $\tilde{\psi}(t)$. This measure is the H_∞ norm of the error system:

$$||\mathbf{A} - \mathbf{A}_k||_\infty = \sup_\omega ||\mathbf{R}(\omega) - \tilde{\mathbf{R}}(\omega)||_2 \,, \tag{22}$$

in which the resolvent of the full system, $\mathbf{R}(\omega)$, is defined as $\mathbf{R}(\omega) = (i\omega\mathbf{I} - \mathbf{A})^{-1}$ and the resolvent of the full order projection of the reduced system is $\tilde{\mathbf{R}}(\omega) = \mathbf{X}\,(i\omega\mathbf{I}_k - \mathbf{A}_k)^{-1}\mathbf{Y}^\dagger$. It is to be recalled that the L_2 norm of a matrix, denoted as $||\cdot||_2$, is equal to its largest singular value.

Assuming the Hankel singular values have been ordered decreasing in magnitude, it can be shown that the error in the H_∞ norm (22) of the balanced approximation of the full system by any k order system $\mathbf{A}_k$ satisfies the inequality:

$$h_{k+1} \le ||\mathbf{A} - \mathbf{A}_k||_\infty \le 2 \sum_{i=k+1}^{N} h_i \tag{23}$$

where h_{k+1} is the first neglected Hankel singular value (Zhou and Doyle, 1998). Although h_{k+1} is only a lower bound on the error, we have found in examples that this lower bound is nearly attained.

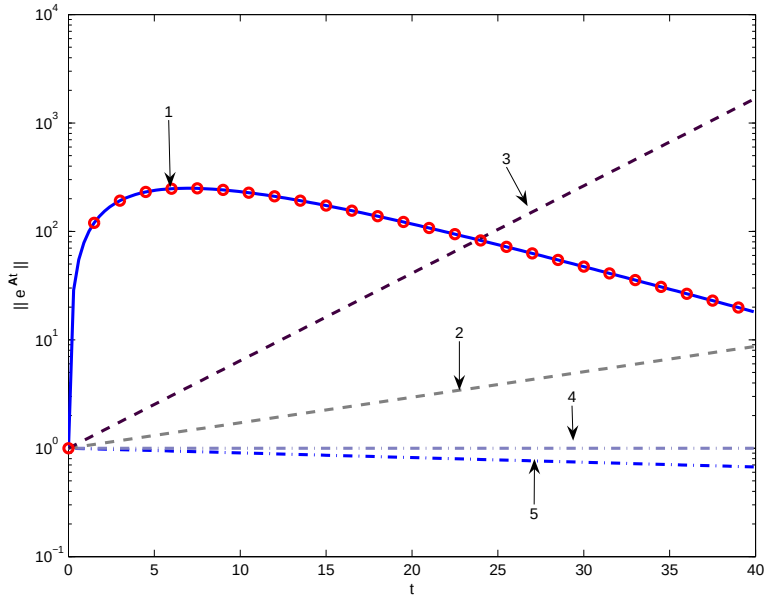

Figure 2: The norm of the propagator $||e^{\mathbf{A}t}||$ as a function of time for the various order 2 approximations of the dynamics. Curve 1: the optimal growth of the original system (24). The circles are the optimal growth of the order 2 system obtained with balanced truncation. This reduced system captures accurately the optimal growth of the full 3×3 system. Curve 2: the optimal growth obtained from a 2×2 truncation obtained by Galerkin projection on the two optimal vectors associated with the two largest singular values of the propagator for time $t=5$. The order 2×2 operator that results is unstable. Curve 3: same as 2 but the optimal vectors are obtained for time $t=3$. Curve 4: the optimal growth obtained from 2×2 truncations obtained by Galerkin projections on the two eigenvectors associated with the two largest eigenvalues of the covariance matrix $\mathbf{P}$ or the matrix $\mathbf{Q}$ (both truncations give identical growths). Curve 5: the optimal growth obtained from a 2×2 truncation obtained by a Galerkin projection on the two least damped eigenmodes of the matrix $\mathbf{A}$. The performance of all the truncated systems, except the one obtained, by balanced truncation is very poor.

3.1 A simple example of balanced truncation

Consider the 3×3 dynamical system:

$$\frac{d\psi}{dt}=\mathbf{A}\psi\ , \tag{24}$$

with

$$\mathbf{A}=\begin{pmatrix}-0.1 & 100 & 0\\ 0 & -0.2 & 0\\ 0 & 0 & -0.01\end{pmatrix}\ . \tag{25}$$

This system is stable but highly non-normal in the first coordinates whilst its third coordinate, which when excited decays the slowest, does not interact with the other coordinates. The non-normality of the system leads to substantial optimal growth as revealed by the norm of the propagator, $||e^{\mathbf{A}t}||$, which measures the maximum state norm that can be produced at time t, by initial states of unit norm. The optimal growth as a function of time is shown in Fig. 2. We wish to obtain a 2×2 system that best approximates the dynamics of the original system.

We first obtain a 2×2 order reduction by Galerkin projection on the two least damped eigenmodes $\mathbf{e}_1$, $\mathbf{e}_2$ of

A. This is achieved as follows: form the 3×2 matrix

$$\mathbf{E} = [\mathbf{e}_1, \mathbf{e}_2] \,, \tag{26}$$

and the 2×2 diagonal matrix $\mathbf{D}_2$ with diagonal elements the first two least damped eigenvalues of **A**. The 2×2 reduced order matrix in coordinates that preserve the original state norm is

$$\mathbf{A}_{2,m} = \mathbf{M}^{1/2} \mathbf{D}_2 \mathbf{M}^{-1/2} \,, \tag{27}$$

where $\mathbf{M} = \mathbf{E}^\dagger \mathbf{E}$. The performance of the norm of the propagator of the modally reduced system as a function of time is shown in Fig. 2 (curve 5), and clearly this truncation provides a very poor representation of the dynamics.

We obtain next a 2×2 order reduction by Galerkin projection on the top two singular vectors of the propagator at time $t = 5$ when the global optimal growth is achieved. This reduction is achieved as follows: form the matrix

$$\mathbf{V} = [\mathbf{v}_1, \mathbf{v}_2] \,, \tag{28}$$

where $\mathbf{v}_1$, $\mathbf{v}_2$ are the singular vectors, and then the matrix $\mathbf{A}_1 = \mathbf{V}^\dagger \mathbf{A} \mathbf{V}$, which is the matrix representation in the coordinates ϕ, in which $\psi = \mathbf{U}\phi$. Then the 2×2 reduction in this basis is the top 2×2 submatrix of $\mathbf{A}_1$. Because the basis vectors are orthonormal the square norm of the transformed states ϕ is equal to the square norm of the original states. This procedure can be followed to obtain order reduction by Galerkin projection on any set of orthonormal vectors. The performance of the reduced system in this basis is poor, as shown in Fig. 2 (curve 2). Note that the reduced order system is unstable. Selecting as a basis the singular vectors for time $t = 3$ leads to even worse performance (curve 3 in Fig. 2). The same results would have been obtained if we had used as a basis the corresponding evolved optimals (the left singular vectors). In general it is found that if the singular vectors are used for order reduction it is best to use the singular vectors or the evolved optimals for a sufficiently long time. Short time optimals can be very suboptimal as a basis for truncation, because these vectors are often associated with directions of rapid growth that does not persist.

We reduce the order of the system by Galerkin projection on the top two eigenvectors of the covariance matrix **P**. The performance is very poor (see Fig.2, curve 4). The same poor performance is obtained if we use the top two eigenvectors of the covariance matrix **Q**. The reason for the failure is that the controllability ellipsoid $\mathbf{x}^T \mathbf{P}^{-1} \mathbf{x} = 1$ is elongated in the direction of $\psi = [1, 10^{-3}, 0]^T$ with semi-major axis of about 900. The second largest direction is the normal direction $\psi = [0, 0, 1]^T$ with semi-major axis length of about 7. This second direction is the normal direction, which because of the relatively slow decay persists for a long time when it is excited. The observability ellipsoid $\mathbf{x}^T \mathbf{Q}^{-1} \mathbf{x} = 1$ is elongated in the direction of $\psi = [2 \times 10^{-3}, 1, 0]^T$ with semi-major axis of about 900. The second largest direction is again the normal direction $\psi = [0, 0, 1]^T$ with semi-major axis length of about 7. It is thus clear that retaining the two dominant directions of either the **P** or the **Q** matrix doesn't retain the two dominant directions of both the **P** and the **Q** matrix that are both necessary for a good description of the dynamics.

The transformation

$$\mathbf{X} = \begin{pmatrix} -15.6 & -15.6 & 0 \\ -0.02 & 0.04 & 0 \\ 0 & 0 & 1 \end{pmatrix} \,, \tag{29}$$

and its associated biorthogonal

$$\mathbf{Y} = \begin{pmatrix} -0.04 & -0.020 & 0 \\ -15.6 & 15.5 & 0 \\ 0 & 0 & 1 \end{pmatrix} \,, \tag{30}$$

renders both the covariance matrix $\tilde{\mathbf{P}} = \mathbf{Y}^\dagger \mathbf{P} \mathbf{Y}$ and the stochastic optimal matrix $\tilde{\mathbf{Q}} = \mathbf{X}^\dagger \mathbf{Q} \mathbf{X}$ diagonal and equal to each other. This associated common ellipsoid (Fig. 4) in the balanced coordinates has semi-major axes

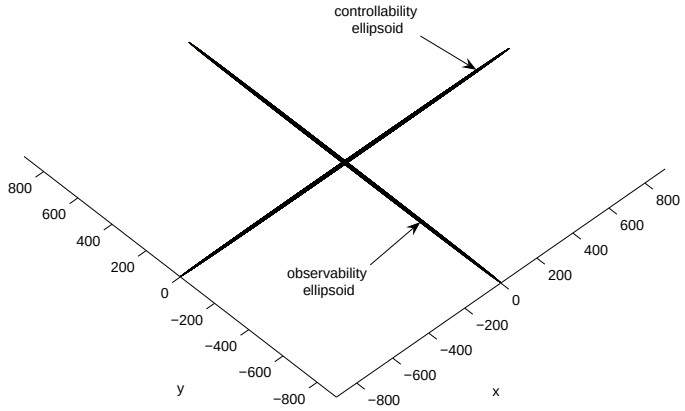

Figure 3: The two ellipsoids associated with the covariance matrix $\mathbf{P}$ *and the stochastic optimal matrix* $\mathbf{Q}$*. The ellipsoids are respectively* $\mathbf{x}^T\mathbf{P}^{-1}\mathbf{x} = 1$ *(the controllability ellipsoid) and* $\mathbf{x}^T\mathbf{Q}^{-1}\mathbf{x} = 1$ *(the observability ellipsoid) and have semi-major axes proportional to the square roots of the eigenvalues of the matrices* $\mathbf{P}$ *and* $\mathbf{Q}$*. The ellipsoids are like needles. The elongated direction of the* $\mathbf{P}$ *ellipsoid indicates that the dominant response of the system is in that direction, while the elongated direction of the* $\mathbf{Q}$ *ellipsoid identifies the forcing directions in which the system responds most readily. These two directions are different. A good reduction of the order of the dynamics must include both of these directions. This is systematically achieved with balanced truncation.*

equal to the square roots of the Hankel singular values, namely approximately equal to 54, 21, 7. Balanced order reduction proceeds in this coordinate system by retaining the two directions that are associated with the two top Hankel singular values, which are to a very good approximation the first and second direction. In this way the reduced order 2×2 balanced system includes the dominant directions of both the controllability and observability ellipsoids and is expected to be a near optimal reduction of order. This is shown in Fig. 2 in which the circles that give the optimal growth of the propagator of the balanced system reproduces exactly the optimal growth of the original system. However, the accuracy of the reduced system can be best examined by considering the difference of the exact and reduced systems by evaluating the norm of the difference of the resolvents of the two systems as a function of frequency ω. This difference is plotted as a function of frequency in Fig. 5. The maximum of this difference over all frequencies defines the H_∞ norm of the error which has been shown to satisfy inequality (31), which in this case becomes:

$$50 \;\leq\; ||\mathbf{A} - \mathbf{A}_2||_\infty \;\leq 100\,, \tag{31}$$

given that the neglected Hankel singular value is $h_3 = 50$. The error system is found in this way to perform worst at $\omega = 0$ when forced with the structure of the neglected persistent mode $[0,0,1]^T$.

4 Applying balanced truncation to the mean storm track perturbation model

In order to obtain a balanced truncation of the storm track model governed by operator (6) we first obtain the covariance matrix, $\mathbf{P}$, and the stochastic optimal matrix, $\mathbf{Q}$, by solving Lyapunov equations (8) and (15) respectively. The eigenfunction of $\mathbf{P}$ associated with the largest eigenvalue is the first EOF of the perturbation

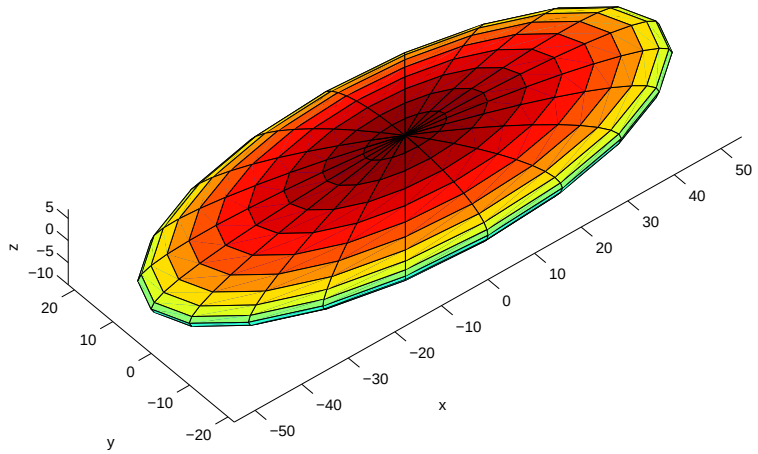

Figure 4: The ellipsoid of the **P** *and* **Q** *matrices in the balanced coordinates. These coordinates are constructed so that the transformed covariance and the optimal matrix ellipsoids become identical. In these coordinates the system can be most effectively truncated because the directions of the system's dominant response coincide with the directions in which the system is most easily forced . The length of the semi-major axes of this ellipsoid are the square roots of the Hankel singular values.*

field, and the eigenfunction of **Q** associated with the largest eigenvalue is the first SO of the perturbation field. The structure of the first EOF, which accounts for 23 % of the streamfunction perturbation variance, is concentrated in the exit region of the storm track as can be seen in Fig. 6 (top left panel). By contrast, the first SO, which is responsible for generating 19.7 % of the streamfunction perturbation variance, is concentrated at the entrance region of the storm track and is nearly orthogonal to the first EOF as can be also seen in Fig. 6 (bottom left panel). This near orthogonality between the EOF structures and SO structures remains even at order 30. Balanced truncation accomplishes an accurate representation of the dynamics by retaining both the structure of the dominant EOF's and of the SO's. It is clear from Fig. 6 that truncations based on projections on the leading EOF's will be very suboptimal as the leading EOF's span well only perturbations concentrated in the exit region of the storm track, leaving the dynamically important entry region of the storm track, where perturbations have greatest potential growth , virtually without support in the span of the retained basis.

Although the error in the frequency response of a balanced truncation (cf (31)) is bounded above by twice the sum of the neglected Hankel singular values and below by the first neglected Hankel singular value, experience shows balanced truncation of tangent linear forecast error systems results in truncation errors close to the lower bound. The Hankel singular values and the eigenvalues of **P** and the **Q** for the storm track model are shown in Fig. 7.

Note that the decrease with mode number of the eigenvalues of **P** and of **Q** is more rapid than that of the Hankel singular values. But this more rapid decrease with mode number of the eigenvalues of **P** and **Q** does not indicate the order required for an accurate approximation; this is instead determined by the first neglected Hankel singular value which falls more slowly with mode number.

It is often assumed that a system can be well approximated by Galerkin projection onto a subspace of its EOF's; with the effectiveness of the truncation being judged from the magnitude of the eigenvalues of the neglected EOF's. This is valid only for normal systems and we see here that for non-normal systems the decrease with

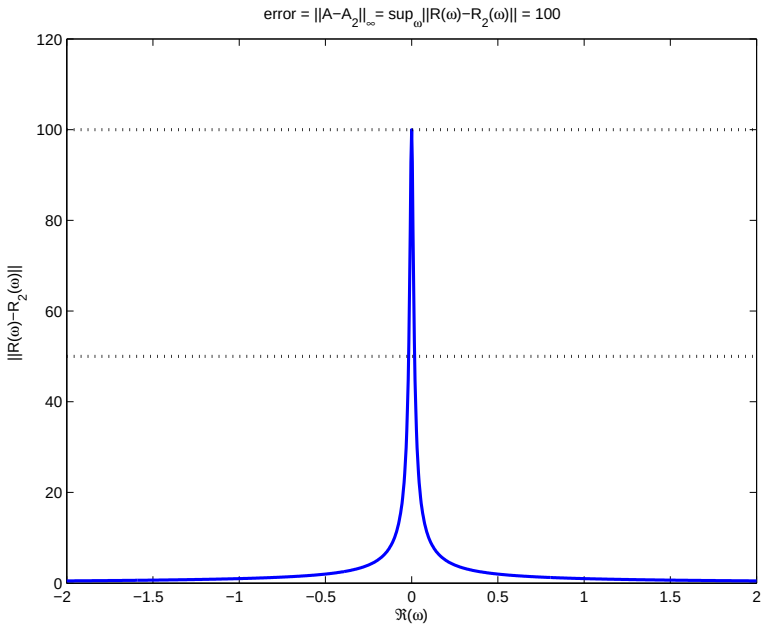

Figure 5: The norm of $||\mathbf{R}(\omega) - \mathbf{R}_2(\omega)||$ *as a function of real frequency,* $\Re(\omega)$*, where* $\mathbf{R}_2(\omega) = \mathbf{X}(i\omega\mathbf{I}_2 - \mathbf{A}_2)^{-1}\mathbf{Y}^\dagger$ *is the resolvent of the* 2×2 *system obtained from balanced truncation. This maximum of this norm over all frequencies defines the* H_∞ *norm of the error system, which provides the greatest error that can be produced in the truncated system when it is forced by monochromatic sinusoidal forcing. The two horizontal lines indicate the bounds that the balanced truncation error must satisfy in this measure. The lower dotted line is the first neglected Hankel singular value* $h_3 = 50$*, the top is* $2h_3$*. The* H_∞ *norm of the error assumes the upper bound of inequality (31). This error is realized when the system is forced at zero frequency (*$\omega = 0$*) with the structure of the most persistent mode of the system* $[0, 0, 1]^T$*.*

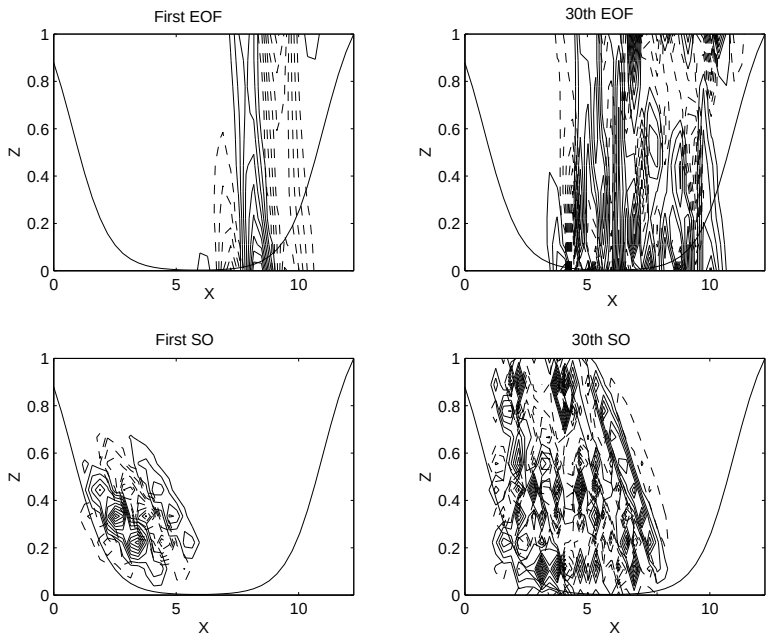

Figure 6: For the stable time mean storm track model. Top panels: The streamfunction of the first and the 30th EOF. The first EOF accounts for 23 % of the maintained variance, the 30th EOF accounts for 0.35 % of the variance. Bottom panels: The structure of the streamfunction of the first and 30th Stochastic Optimal. The first SO is responsible for producing 19.7 % of the maintained variance; the 30th SO is responsible for producing 0.48 % of the maintained variance.

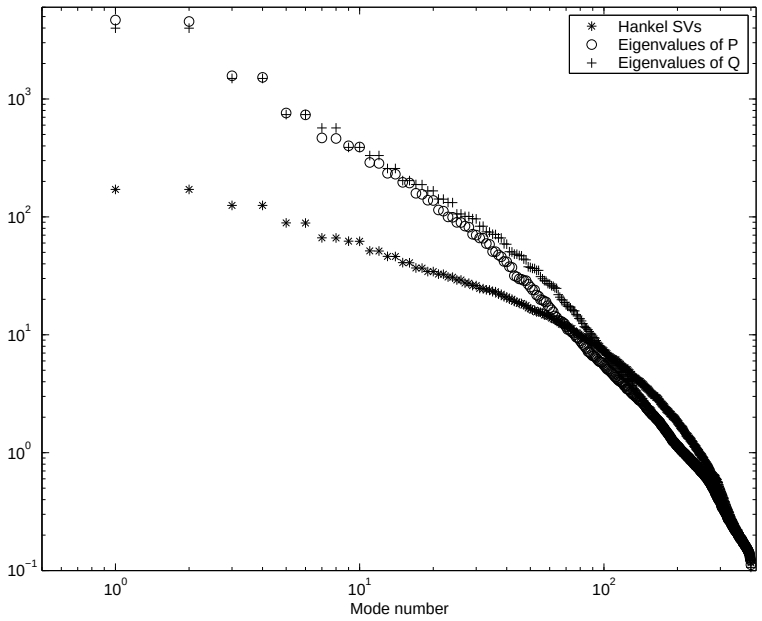

Figure 7: The Hankel singular values (stars) compared to the eigenvalues of the covariance matrix **P** *(circles), and the eigenvalues of the stochastic optimal matrix* **Q** *(crosses). The Hankel singular values are the square roots of the eigenvalues of the product* **PQ**. *Note that the EOF's (the eigenvalues of* **P***) and the SO's (the eigenvalues of* **Q***) fall much more rapidly with mode number than do the Hankel singular values.*

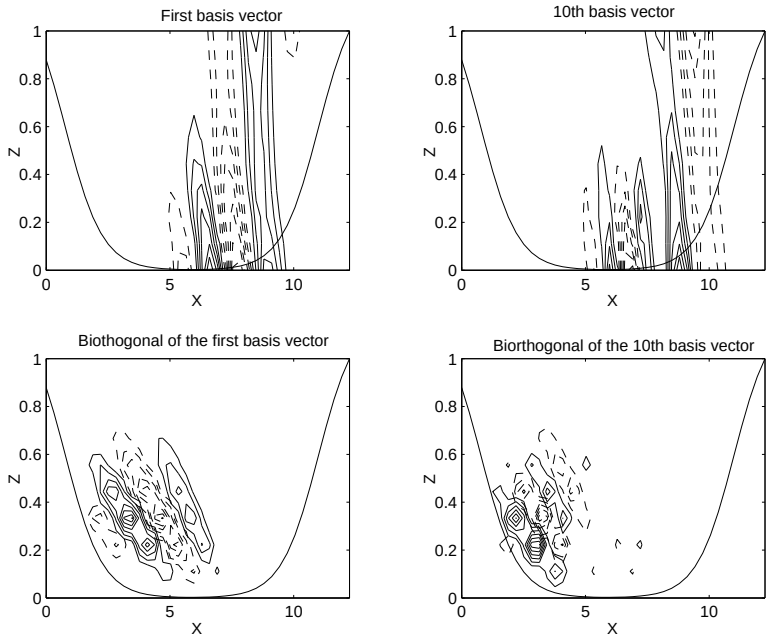

Figure 8: For the stable time mean storm track model. Top left panel: the streamfunction of the first basis vector of the expansion for the balanced truncation of the system. It is given by the first column of **X**. *Top right panel: the streamfunction of the tenth basis vector of the expansion for the balanced truncation of the system. It is given by the tenth column of* **X**. *Bottom left panel: the streamfunction of the biorthogonal of the first basis vector. It is given by the first column of* **Y**. *Bottom right panel: the streamfunction of the tenth basis vector. It is given by the tenth column of* **Y**.

mode number of the eigenvalues of the covariance matrix is misleading and generally optimistic even as an estimate of the order of the system required for an accurate approximation.

A subset of the columns of **X** is retained in the balanced truncation. This non-orthogonal basis and its biorthogonal, the columns of **Y**, are constructed so as to capture the structures supporting the dynamics most efficiently, simultaneously accounting for the preferred responses (EOF's) and the preferred excitations (SO's) of the dynamics. The first and the tenth structure retained in the dynamics (the first and the tenth column of **X**) and their biorthogonal structures (the first and tenth column of **Y**) are shown in Fig. 8.

The storm track model and its reduced order approximate have very different eigenvalue spectra. The eigenvalue spectrum of the reduced order approximate is such that the frequency response of the approximate system is as close as possible to that of the original system, which is shown in Fig. 9. This results both from a decrease in the stability of the reduced system compared to that of the full system and from the increase in growth due to the non-normality in the reduced system.

The accuracy of the approximation is measured by the H_∞ norm of the error dynamical system $||\mathbf{A}-\mathbf{A}_{60}||_\infty$, which, as discussed in the previous section, lies between the lower bound given by the first neglected Hankel singular value, $h_{61} = 13.8$, and the upper bound: $2\sum_{i=61}^{400} h_i = 1.8\times 10^3$. The largest singular value of the error system resolvent as a function of frequency is shown in Fig. 10, where it can be seen that $||\mathbf{A}-\mathbf{A}_{60}||_\infty = 28.5$, which shows that the balanced truncation error in this example is only approximately twice its lower bound. The error is nearly white for the span of frequencies that correspond to the frequencies of the system eigenmodes. For comparison, the error incurred in an order 60 Galerkin projection of the dynamics onto the first 60 EOF's and the error incurred in an order 60 Galerkin projection onto the first 60 least damped modes, are also shown in Fig. 10. It can be seen that the EOF projection performs appreciably worse than the balanced

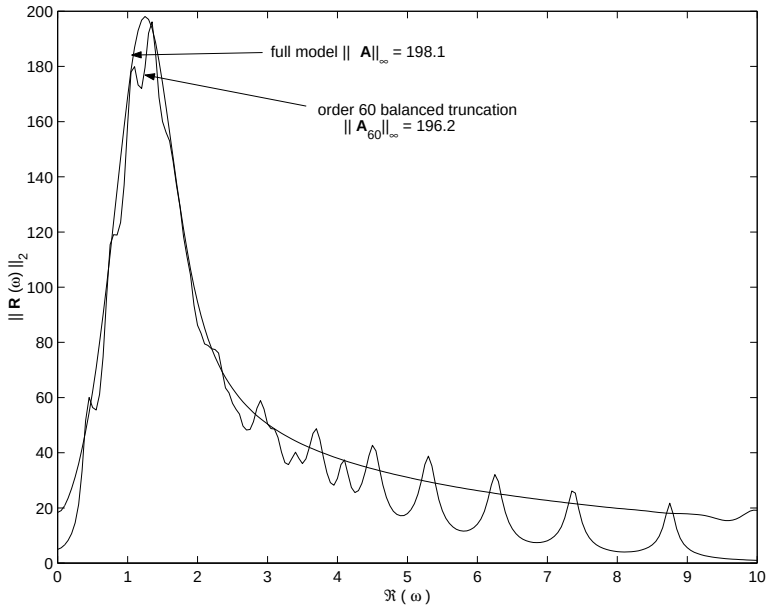

Figure 9: The maximum singular value of the resolvent $\mathbf{R}(\omega) = (i\omega I - \mathbf{A})^{-1}$ *of the full system* $\mathbf{A}$ *as a function of the real frequency,* $\Re(\omega)$*. The maximum of this curves as a function of* ω *is the* H_∞ *norm of* $\mathbf{A}$ *which is found here to be 198.1. Also plotted is the maximum singular value of the resolvent associate with* $\mathbf{A}_{60}$*, which is the operator obtained from an order 60 balanced truncation of* $\mathbf{A}$*. The maximum of this curves is the* H_∞ *norm of* $\mathbf{A}_{60}$ *which is found to be 196.2.*

truncation, while the modal truncation at this order is useless.

The optimal growth[2] as a function of optimizing time attained by the full system and by the following: the order 60 balanced truncation; the order 60 system obtained by Galerkin projection on the first 60 EOF's; the order 60 system obtained by Galerkin projection on the first 60 SO's; and the order 60 system obtained by Galerkin projection on the first 60 least damped modes are all shown in Fig. 11. Note that the balanced truncation performs very well, reproducing the optimal growth nearly perfectly up to $t = 5$, corresponding to about 2 days. By comparison the EOF and SO truncations perform appreciably worse and the modal truncation gives even poorer results.

The structure of the initial perturbation that leads to greatest square streamfunction growth at $t = 10$ in the full system, together with the resulting structure, is shown in Fig. 12; for comparison these structures as obtained by the truncated system are also shown. The structures are well captured by the order 60 reduced system.

We have demonstrated how to obtain balanced truncation of a stable time independent system but the method of balanced truncation can be extended to unstable systems (Sznaier et al, 2002) and to time dependent systems in which balancing is performed sequentially over finite time intervals (Van Dooren, 2000).

In forecast applications we seek an accurate reduction of the dynamics of the time dependent tangent linear operator calculated on the system trajectory over a limited time interval (24 or 48 hours). One choice is to balance on the time mean operator over this interval. Another choice is to balance on the time dependent version of the tangent linear operator over this or an extended interval about the assimilation time, obtaining approximation of the $\mathbf{P}$ and $\mathbf{Q}$ matrices on this interval. Both procedures have been tested using the time dependent version of our storm track model and found to produce accurate truncations. We examine below

[2] The optimal growth at time, t, is defined as the maximum perturbation growth that can occur over time t. For an autonomous system, governed by $\mathbf{A}$, the optimal growth at t is given by the largest singular value of $e^{\mathbf{A}t}$ or by $||e^{\mathbf{A}t}||_2$.

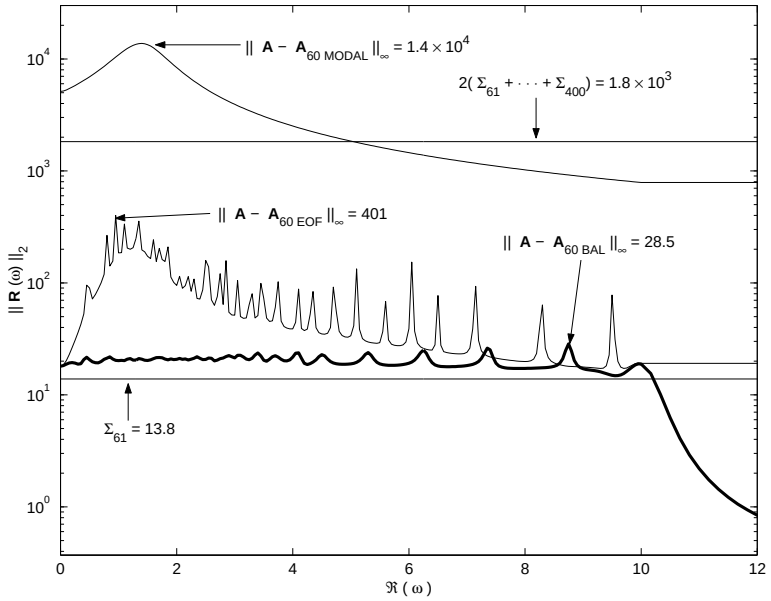

Figure 10: For the stable time mean storm track model: the maximum singular value of the error system $\mathbf{A}-\mathbf{A}_{60}$ *as a function of real frequency,* $\Re(\omega)$*. The system* $\mathbf{A}_{60}$ *is an order 60 approximation obtained from* $\mathbf{A}$ *by balanced truncation. The maximum of this curves is the* H_∞ *error of the order 60 balanced truncation which is found here to be 28.5. Also indicated with a straight line is the theoretical minimum error of an order 60 truncation, which equals the first neglected Hankel singular value* $\Sigma_{61} = 13.8$*. The balanced truncation is seen to be nearly optimal.*

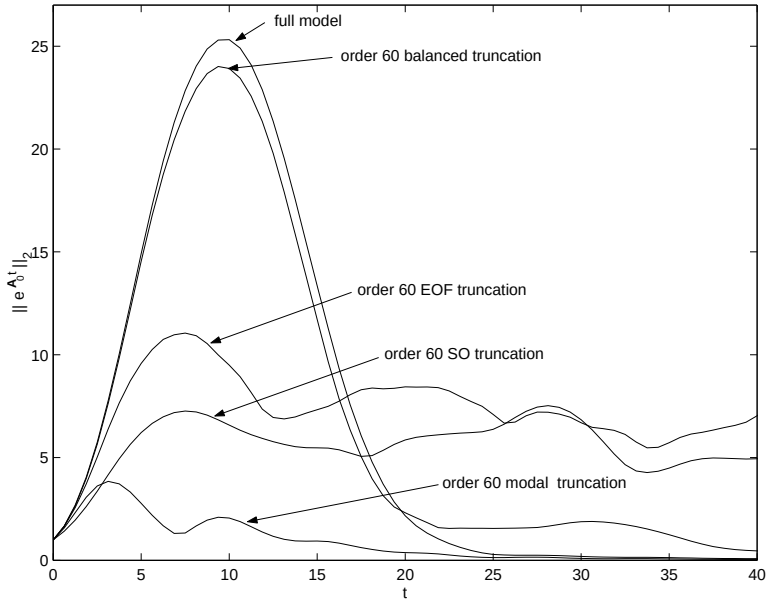

Figure 11: Optimal growth, $||e^{\mathbf{A}t}||$*, as a function of time for the Eady model in a channel with sponge layers and meridional wavenumber* $l = 1$*. Shown is the optimal growth for the full system with 400 degree of freedom and the optimal growth produced by an order 60 approximate system obtained by balanced truncation of the full system. Shown also for comparison is the optimal growth attained by the order 60 approximate system obtained by Galerkin projection on the first 60 EOF's, the first 60 SO's and the first 60 least damped modes.*

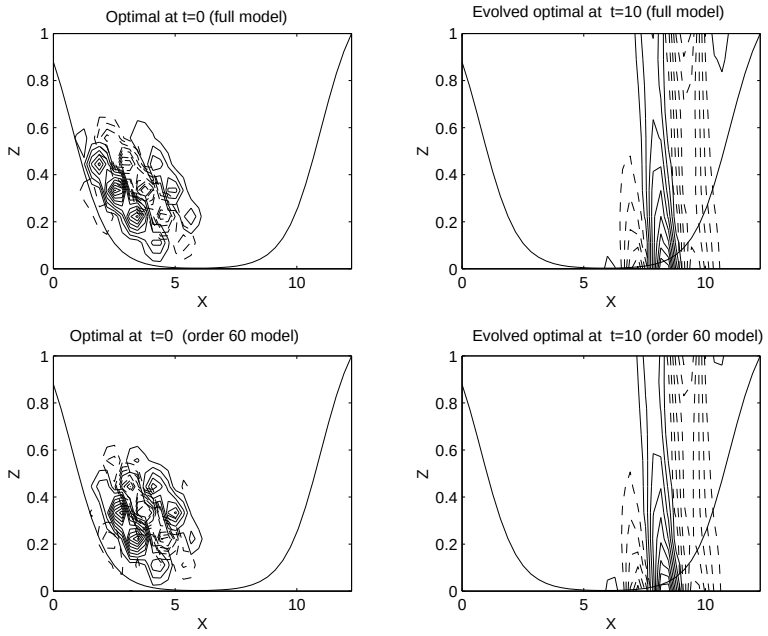

Figure 12: For the stable time mean storm track model. The structure of the streamfunction of the optimal perturbation that leads to the greatest energy growth at $t = 10$ (left panels), and the evolved optimal streamfunction, which is the structure that these optimals evolve into at the optimizing time $t = 10$ (right panels). The top panels are for the full system while the bottom panels are for the order 60 balanced truncation.

results obtained from a reduced order Kalman filter in which the truncation is made on the time dependent tangent linear operator over 48 hours centered on the assimilation time.

The time mean tangent linear operator (the mean being calculated over an interval) is generally asymptotically stable. This is because realistic states of the atmosphere support primarily instabilities with positive group velocities and do not support absolute instabilities (unstable modes with zero group velocity)(Farrell, 1982; Lin and Pierrehumbert, 1993; DelSole and Farrell, 1994). The asymptotic instability of the tangent linear system arises primarily from the continual instigation of transient growth which occurs in non periodic time dependent systems in the same way that the Mathieu instability arises in time periodic systems. This mechanism is discussed in Farrell and Ioannou (1999) and has been verified in the context of a forecast system by Reynolds and Errico (1999) and Gelaro et al (2000). The stability of the mean operator allows balancing to be performed on a stable operator although the error system itself is nonautonomous and asymptotically unstable. However, it is not necessary to balance on the mean operator, and as remarked above comparable results can be obtained by balancing on the time dependent tangent linear operator over an appropriate interval; experiment suggests approximately 48 hours.

5 Assimilation as an observer system

Consider assimilating data taken from truth, $\mathbf{x}_t$. The forecast error $\mathbf{e}_f = \mathbf{x}_f - \mathbf{x}_t$ obeys the equation:

$$\frac{d\mathbf{e}_f}{dt} = \mathbf{A}\mathbf{e}_f + \mathbf{Q}^{1/2}\mathbf{w}_m \,, \tag{32}$$

in which $\mathbf{A}$ is the unstable tangent linear operator, $\mathbf{Q}$ is the model error covariance, and w_m is assumed to be a vector of temporally uncorrelated noise processes.

Introduce n observations, $\mathbf{y}_{ob}$, obtained from truth $\mathbf{x}_t$ as:

$$\mathbf{y}_{ob} = \mathbf{H}\mathbf{x}_t \; + \; \mathbf{R}^{1/2}\mathbf{w}_o \; , \tag{33}$$

where $\mathbf{H}$ is the observation matrix, $\mathbf{R}$ is the observational error covariance and $\mathbf{w}_o$ is an n vector of white noise processes.

Assimilate these observations to obtain an analysis, x_a, with analysis error $\mathbf{e}_a = \mathbf{x}_a - \mathbf{x}_t$ satisfying the Luenberger observer system:

$$\begin{aligned} \frac{d\mathbf{e}_a}{dt} &= \mathbf{A}\mathbf{e}_a + \mathbf{K}(\mathbf{y}_{ob} - \mathbf{H}\mathbf{x}_a) + \mathbf{Q}^{1/2}\mathbf{w}_m \\ &= (\mathbf{A} - \mathbf{K}\mathbf{H})\mathbf{e}_a + \mathbf{K}\mathbf{R}^{1/2}\mathbf{w}_o + \mathbf{Q}^{1/2}\mathbf{w}_m \; . \end{aligned} \tag{34}$$

The gain, $\mathbf{K}$, is chosen to minimize the analysis error variance trace$(< \mathbf{e}_a\mathbf{e}_a^\dagger >)$. Unlike the forecast error system, a Luenberger observer system is asymptotically stable. Any gain, $\mathbf{K}$, that stabilizes the tangent linear operator results in an observer with bounded error, this error being forced by a combination of model error $\mathbf{Q}$ and observational error $\mathbf{R}$ (cf 34). Good gains do not just stabilize the operator but simultaneously reduce the non-normality of the tangent linear operator so that the minimum of trace$(< \mathbf{e}_a\mathbf{e}_a^\dagger >)$ is maintained by the combination of observational and model error.

Just as generalized stability of the tangent linear forecast system reveals the potential for forecast failures due to transient growth of initialization error or unresolved forcings distributed over the forecast interval, so also does generalized stability analysis of the observer system reveal how model error and initialization error contribute to analysis failures.

5.1 The case of an optimal observer

The gain $\mathbf{K}$ that minimizes the statistical steady analysis error variance trace$(< \mathbf{e}_a\mathbf{e}_a^\dagger >)$ is the Kalman gain. For simplicity of presentation we take as our example an operator $\mathbf{A}$ that is time independent and observations taken continuously in time. A stationary error system with continuous observations is chosen for heuristic reasons although in forecast systems the tangent linear operator is time dependent and observations are introduced at discrete intervals. However, the statistical properties of optimal state estimation are general and results are qualitatively similar across observer systems.

The asymptotic Kalman gain resulting from continual assimilation of observations with observation matrix $\mathbf{H}$ is:

$$\mathbf{K} = \mathbf{P}\mathbf{H}^\dagger\mathbf{R}^{-1} \; , \tag{35}$$

with $\mathbf{P}$ the stabilizing solution of the algebraic Ricatti equation:

$$\mathbf{A}\mathbf{P} + \mathbf{P}\mathbf{A}^\dagger - \mathbf{P}\mathbf{H}^\dagger\mathbf{R}^{-1}\mathbf{H}\mathbf{P} + \mathbf{Q} = 0 \; . \tag{36}$$

It is a property of the Kalman filter that the matrix $\mathbf{P}$ obtained as a solution of the algebraic Riccati equation is also the asymptotic error covariance of the observer system (34).

5.2 4D-Var as an observer system

4D-Var data assimilation with assimilation window T can be viewed as a special case of an observer in which a climatological background error covariance $\mathbf{B}$ is advanced for T units of time. In our autonomous model system the error covariance is advanced according to:

$$\mathbf{P} = e^{\mathbf{A}T}\mathbf{B}e^{\mathbf{A}^\dagger T} \; , \tag{37}$$

from which we obtain the gain:

$$\mathbf{K}_{4D-Var} = \mathbf{P}\mathbf{H}^\dagger(\mathbf{H}\mathbf{P}\mathbf{H}^\dagger + \mathbf{R})^{-1} \ . \tag{38}$$

This gain produces a stabilized observer if enough observations are made.

The asymptotic error in the observer (34) is obtained by calculating the covariance, $\mathbf{P}$, that solves the equation:

$$\left(\mathbf{A} - \mathbf{K}_{4D-Var}\mathbf{H}\right)\mathbf{P} + \mathbf{P}\left(\mathbf{A} - \mathbf{K}_{4D-Var}\mathbf{H}\right)^\dagger + \mathbf{K}_{4D-Var}\mathbf{R}\mathbf{K}_{4D-Var}^\dagger + \mathbf{Q} = 0 \ . \tag{39}$$

6 Effect of the number of observations on the performance of the assimilation

Consider convergence of the assimilated state to truth as more observations are taken in the presence of model error. To fix ideas assume that repeated independent observations are made at each of the grid points of our model.

If the state of the assimilation system has dimension N and n observations are taken at each grid point the observation matrix for these n observations, $\mathbf{H}_n$, is an $nN \times N$ matrix:

$$\mathbf{H}_n = \mathbf{I}_N \bigotimes e \tag{40}$$

where $\mathbf{I}_N$ is the identity N^2 dimensional matrix, $\bigotimes$ denotes the Kronecker product and e is the unit column $e = [1, \cdots, 1]^T$ of dimension n.

Consider an observation error covariance matrix $\mathbf{R} = r\mathbf{I}_N \bigotimes \mathbf{I}_n$, where $\mathbf{I}_n$ is the n^2 dimensional identity matrix and let $\mathbf{K}_n$ be the Kalman gain that results from these n observations. The Kalman gain is:

$$\mathbf{K}_n = \mathbf{P}_n\mathbf{H}_n^\dagger\mathbf{R}^{-1} = \frac{1}{r}\mathbf{P}_n(\mathbf{I}_N \bigotimes e^\dagger), \tag{41}$$

with $\mathbf{P}_n$ the stabilizing solution of the algebraic Ricatti equation:

$$\mathbf{A}\mathbf{P}_n + \mathbf{P}_n\mathbf{A}^\dagger - \mathbf{P}_n\mathbf{H}_n^\dagger\mathbf{R}^{-1}\mathbf{H}_n\mathbf{P}_n + \mathbf{Q} = 0 \ , \tag{42}$$

where $\mathbf{Q}$ is the model error covariance. On substitution of the specific expressions above for the observation matrix $\mathbf{H}_n$ and the observational error covariance matrix $\mathbf{R}$, (42) assumes the simplified form:

$$\mathbf{A}\mathbf{P}_n + \mathbf{P}_n\mathbf{A}^\dagger - \frac{n}{r}\mathbf{P}_n^2 + \mathbf{Q} = 0 \ , \tag{43}$$

from which we conclude that the analysis error in the observer system resulting from assimilation of n observations at each grid point with each observation having observational error variance r is equal to the analysis error that results from observing the same system with a single isolated observation with observational error variance r/n. It remains to determine how the error covariance P_n scales with n.

In the absence of model error ($\mathbf{Q} = 0$) the answer is immediate:

$$\mathbf{P}_n = \frac{\mathbf{P}}{n} \ , \tag{44}$$

where $\mathbf{P}$ is the assimilation error covariance associated with a single observation which satisfies the algebraic Ricatti equation:

$$\mathbf{A}\mathbf{P} + \mathbf{P}\mathbf{A}^\dagger - \frac{1}{r}\mathbf{P}^2 = 0 \ . \tag{45}$$

So in the absence of model error the assimilation square error tends to zero as more observations are taken at the expected rate of n^{-1}.

Consider now the case in which model error exists. In that case we may expand P_n in an asymptotic series:

$$\mathbf{P}_n = \frac{p_o}{\sqrt{n}} + \frac{p_1}{n} + \cdots . \tag{46}$$

The leading term in this expansion is given by:

$$p_o = \sqrt{r}\mathbf{Q}^{1/2} , \tag{47}$$

and consequently the asymptotic error covariance in the presence of model error has the leading behavior:

$$\mathbf{P}_n = \sqrt{\frac{r}{n}}\mathbf{Q}^{1/2}. \tag{48}$$

We conclude that in the presence of model error the assimilation square error of the Kalman filter in our example tends to zero at rate $n^{-1/2}$ as more observations are made.

It is instructive to compare this to the behavior of analysis error in a 4D-Var data assimilation as the number of observations increases. In the absence of model error the 4D-Var analysis square error also tends to zero at rate n^{-1}, but in the presence of model error if the background covariance $\mathbf{B}$ is not rescaled as more observations are taken the analysis error asymptotes to a non zero constant value.

In order to understand this behavior consider the asymptotic error as $n \to \infty$ in the unstable stochastically forced scalar system with growth rate a:

$$\frac{de}{dt} = ae + q^{1/2}w . \tag{49}$$

The associated algebraic Ricatti equation is:

$$2ap_n - \frac{n}{r}p_n^2 + q = 0 , \tag{50}$$

with stabilizing solution:

$$p_n = a\frac{r}{n} + \sqrt{a^2\left(\frac{r}{n}\right)^2 + q\frac{r}{n}} . \tag{51}$$

This stabilizing solution is also the error in the observer system after assimilation of n observations. Note that in the absence of model error and for all n:

$$p_n = \frac{2ar}{n} \quad \text{if } \; q = 0 , \tag{52}$$

and that the Kalman gain is

$$\mathbf{K}_n \; = \; \frac{2a}{n}[1,1,\cdots,1,1] , \tag{53}$$

and that the weight given each in the assimilation is:

$$\mathbf{K}_n\mathbf{H}_n = 2a , \tag{54}$$

indicating that the weight given to observations is proportional to the error growth rate and is independent of the number of observations.

With model error and as $n \to \infty$:

$$p_n \approx \sqrt{\frac{qr}{n}} \quad \text{if } \; q \neq 0 , \tag{55}$$

and the Kalman gain is:

$$\mathbf{K}_n \; \approx \; \sqrt{\frac{q}{rn}}[1,1,\cdots,1,1] , \tag{56}$$

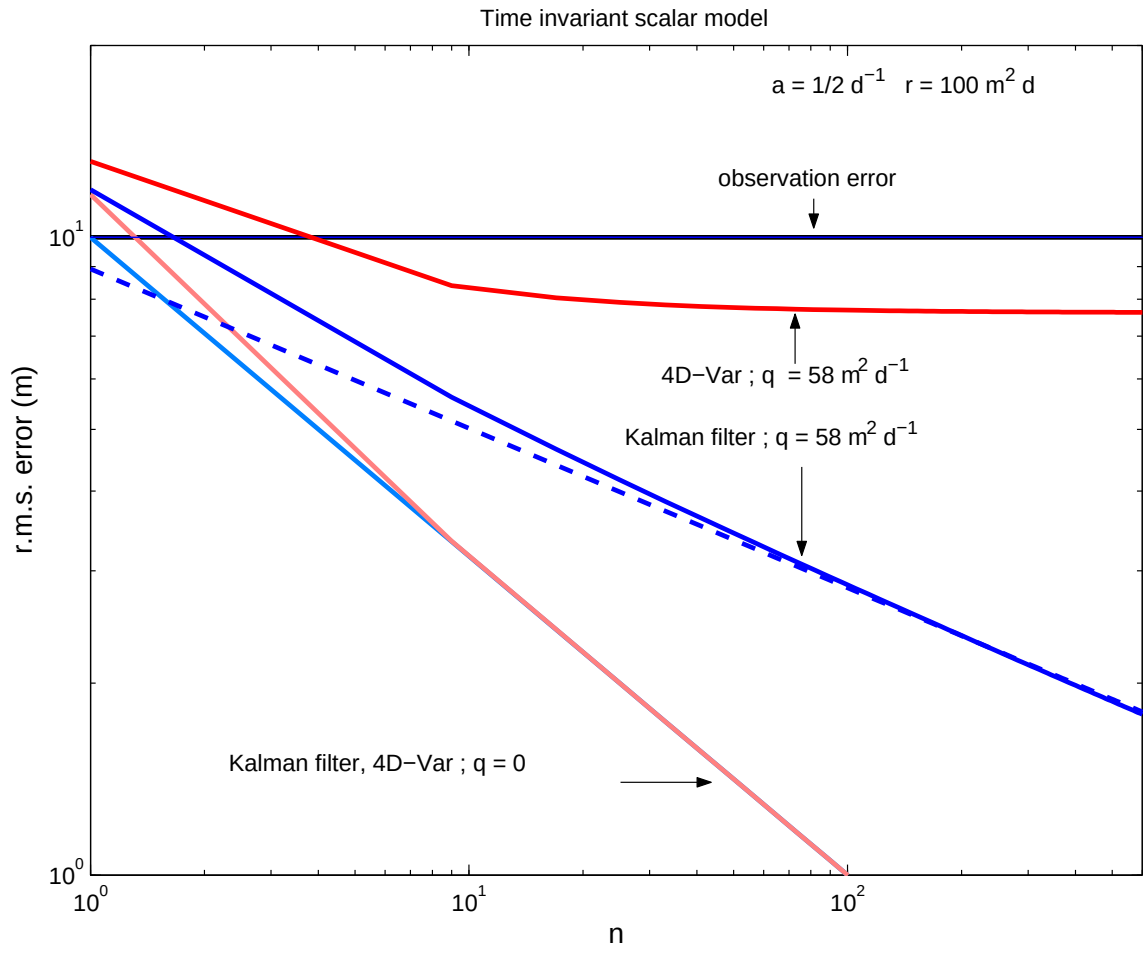

Figure 13: Error in the scalar optimal observer system and a scalar system with an equivalent 4D-Var observer as a function of the number of observations. The gain in the optimal observer is the asymptotic Kalman gain. The growth rate is $a = 1/2\ d^{-1}$, the observational error is 10 m. The model error variance is $q = 58\ m^2\ d^{-1}$ resulting in a model induced error of 10 m after a day. With $q = 0$ the error in both the observer system with the Kalman filter and the 4D-Var falls as $n^{-1/2}$. With $q \neq 0$ the error in the 4D-Var observer asymptotes to a constant value while in the observer with the Kalman filter falls as $n^{-1/4}$.

so that the weight given to observations is:

$$\mathbf{K}_n\mathbf{H}_n = \sqrt{\frac{nq}{r}}\,, \tag{57}$$

independent of error growth rate and indicating that as the number of observations tends to infinity in the presence of model error the model is increasingly discounted and the observations accepted. A comparison of the error as a function of the number of observation in the scalar system is shown in Fig. 13.

Regardless of the model error, the error in the optimal observer vanishes if enough observations are assimilated a result that holds in higher dimensions, as we have seen.

7 Approach of 4D-Var to the Kalman filter as the assimilation interval increases

In the absence of model error 4D-Var is equivalent to the extended Kalman filter if the assimilation window is extended to infinity. Present implementations of 4D-Var employ assimilation windows of 12 hours and it may appear that these implementations must be suboptimal and that the assimilation could be improved by lengthening the assimilation window.

Consider the asymptotic gain arising from a single observation in the time independent storm track model with and without model error. The asymptotic gain is shown in Fig. 14 (top panel). It is evident that in the absence of model error the gain is not localized: the gain identifies the unstable structures of the forecast model and provides loadings designed to destroy these structures which have the character of a global mode. As shown in Fig. 14 (bottom panel) in the presence of model error the gain becomes localized to the neighborhood of the observation because the model error that is distributed in the system produces incoherent responses far from the observation location that cancel when the ensemble average response of the system is taken so that the gain in the presence of model error is localized.

Because 4D-Var calculates the gains without model error the gain associated with a 4D-Var assimilation as the assimilation window is increased extends into the far field. This evolution of the gain associated with an initial climatological background $\mathbf{B}$ in a 4D-Var assimilation is shown in Fig. 15. With time the climatological gain associated with the background error covariance assumes a global structure.

In the absence of model error the gain as the assimilation interval increases approaches the structure of the gain of the Kalman filter and the analysis error of 4D-Var asymptotes to the analysis error obtained by a Kalman filter. The convergence of 4D-Var assimilation error to that of the Kalman filter is shown for the time dependent version of the storm track model in Fig. 16.

However, the perfect model assumption is physically unrealistic, and the 4D-Var assimilation scheme produces gains that have global structure as the assimilation window is increased. We find in our model storm track that 4D-Var performs best with an assimilation window that is large enough to allow the gain to be affected by the flow but short enough so that far-field loadings do not have time to form. An example of 4D-Var analysis error as a function of the assimilation interval is shown in Fig. 17. In this example the optimal assimilation interval is 36 hours.

We conclude that neglect of model error in the formulation of 4D-Var makes 4D-Var operate best for rather short assimilation intervals. Model error must be introduced to make 4D-Var an optimal observer. In the sequel we propose a method for introducing model error into 4D-Var.

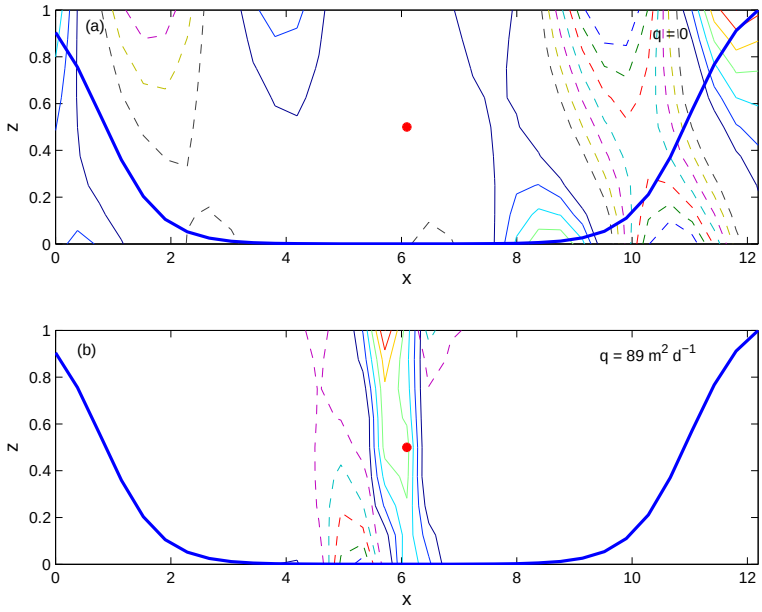

Figure 14: The asymptotic Kalman gain for observation at the center of the channel in the storm track model. Top panel the gain for the case of no model error. Bottom panel the gain for the case with model error. The model error q produces an r.m.s. model error of 5 *m in a day. The r.m.s. observational error is* 10 *m. The asymptotic Kalman gain has been calculated for the time mean flow. Note that the model error leads to localization of the gain in the neighborhood of the observations.*

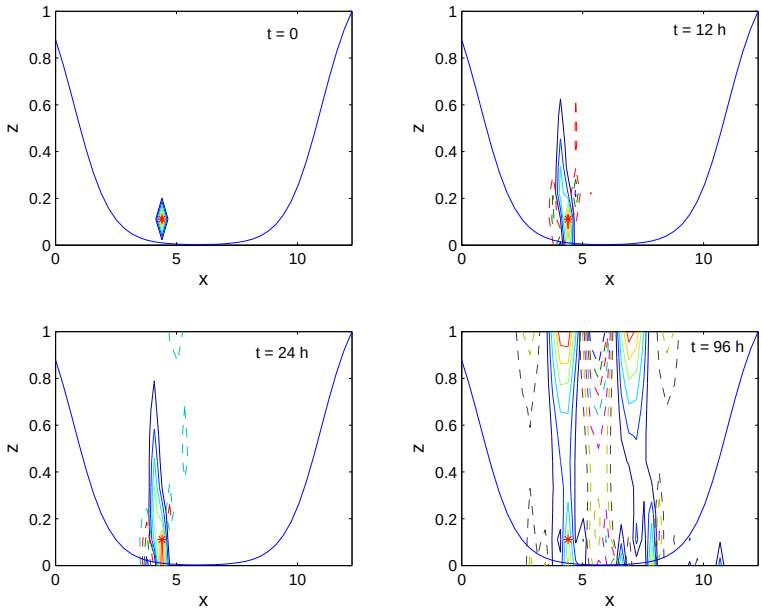

Figure 15: Evolution of the gain associated with the observation marked with a star in 4D-Var as a function of the assimilation interval in the unstable time mean storm track error model. The background **B** *matrix is the identity. As the assimilation interval increases 4D-Var gains extend into the far field.*

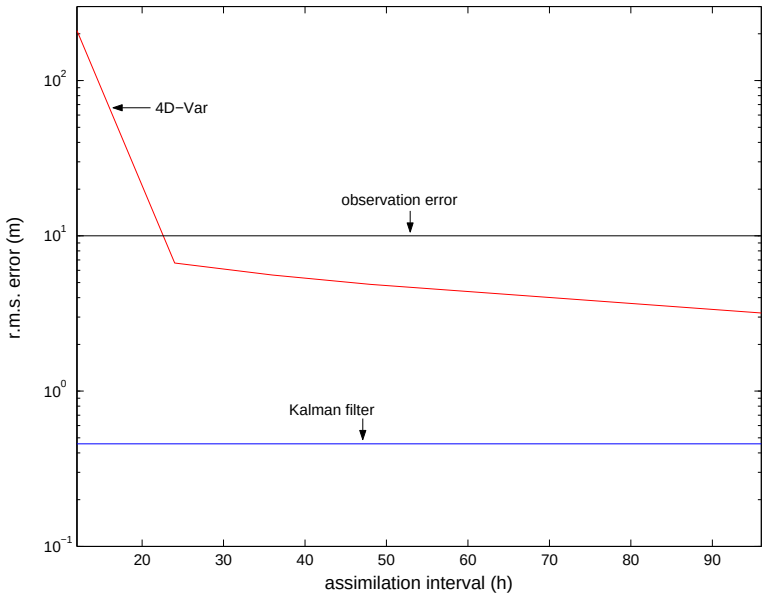

Figure 16: Error in 4D-Var assimilations in the time dependent storm track model with no model error as a function of assimilation interval. Also shown is the error obtained with sequential application of a Kalman filter. 16 observations are assimilated with r.m.s. observational error of 10 *m. As the assimilation interval tends to infinity the 4D-Var error approaches that of the Kalman filter.*

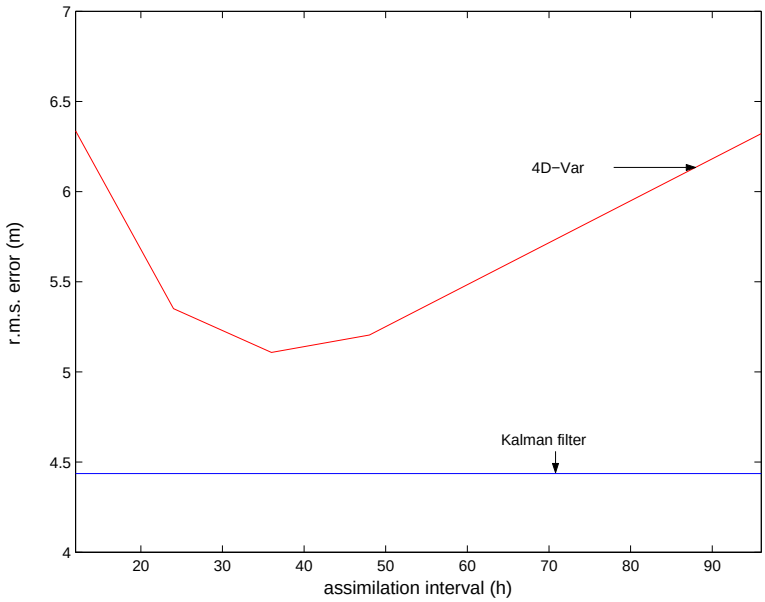

Figure 17: R.m.s. error in 4D-Var assimilations in the time dependent storm track model with model error as a function of assimilation interval. The best 4D-Var performance is achieved in this example for assimilation over the interval 36 *h. Also shown is the error obtained with the Kalman filter. 40 observations are assimilated with r.m.s. observational error of* 10 *m; the model error variance is* $q = 12\ m^2\ d^{-1}$*, so that a model error of* 5 *m accumulates in one day.*

8 Reduced order error covariance estimate

We now formulate the observer system in which the error covariance is advanced in the truncated space to obtain a reduced order Kalman gain. The resulting observer system in reduced coordinates is:

$$\frac{d\mathbf{e}_k}{dt} \;=\; \left(\mathbf{A}_k - \mathbf{K}_k\mathbf{H}_k\right)\mathbf{e}_k + \mathbf{K}_k\mathbf{R}_k^{1/2}\mathbf{w}_o - \mathbf{Q}_k^{1/2}\mathbf{w}_m \;. \tag{58}$$

where the reduced analysis is $\mathbf{e}_k = \mathbf{Y}^\dagger\mathbf{e}_a$ for $k << N$ and the reduced $k \times k$ operator is:

$$\mathbf{A}_k \;=\; \mathbf{Y}^\dagger\mathbf{A}\mathbf{X} \;. \tag{59}$$

The n observations, y_{ob}, are assimilated in the reduced space according to:

$$\mathbf{y}_{ob} = \mathbf{H}_k\mathbf{x}_k \;+\; \mathbf{R}^{1/2}\mathbf{w}_o \;, \tag{60}$$

where the reduced order observation matrix is:

$$\mathbf{H}_k \;=\; \mathbf{H}\,\mathbf{X} \;. \tag{61}$$

The error system in the reduced space is used to obtain the Kalman gain $\mathbf{K}_k$ and to propagate the error covariance,

$$\mathbf{P}_k = < \mathbf{e}_k\mathbf{e}_k^T > \;. \tag{62}$$

The error covariance of the full system is then approximated from that of the reduced covariance $\mathbf{P}_k$ by:

$$\mathbf{P} = \mathbf{X}\mathbf{P}_k\mathbf{X}^\dagger \;. \tag{63}$$

This error covariance is used in our 4D-Var model. By introducing this covariance in 4D-Var we evolve the error covariance and simultaneously also introduce model error. Introduction of this reduced order covariance in 4D-Var makes the 12 hour 4D-Var perform nearly optimally. Analysis of the performance of this filter is shown in Fig. 18. Using the reduced order covariance obtained without model error leads to degradation of the 4D-Var assimilation due to unrealistic far field loadings in the gains.

9 Conclusions

A data assimilation system combines observations and dynamics expressed through a numerical forecast model to obtain an estimate of the state of the atmosphere. An optimal data assimilation system combines observations and dynamics to obtain the statistically best state estimate. Statistical optimality requires information about the observation error and about the error in the numerical forecast. This latter is difficult to obtain because of the high dimension of the error system so that approximations to the forecast error have to be made to implement practical applications of optimal state estimation. A promising method for obtaining an approximation to forecast error is to advance the error covariance in a state space of reduced dimension compared with that of the full forecast error system. The error covariance in the reduced space can then be used in an approximate optimal state estimation method such as 4D-Var or the extended Kalman filter. Such a reduction is possible because the significantly unstable subspace of the error system is of much lower dimension than the complete state dimension.

Assimilation systems can be usefully modelled as observer systems in which any gain matrix that stabilizes the analysis error system is an observer and the gain that results in minimum analysis error is the optimal observer.

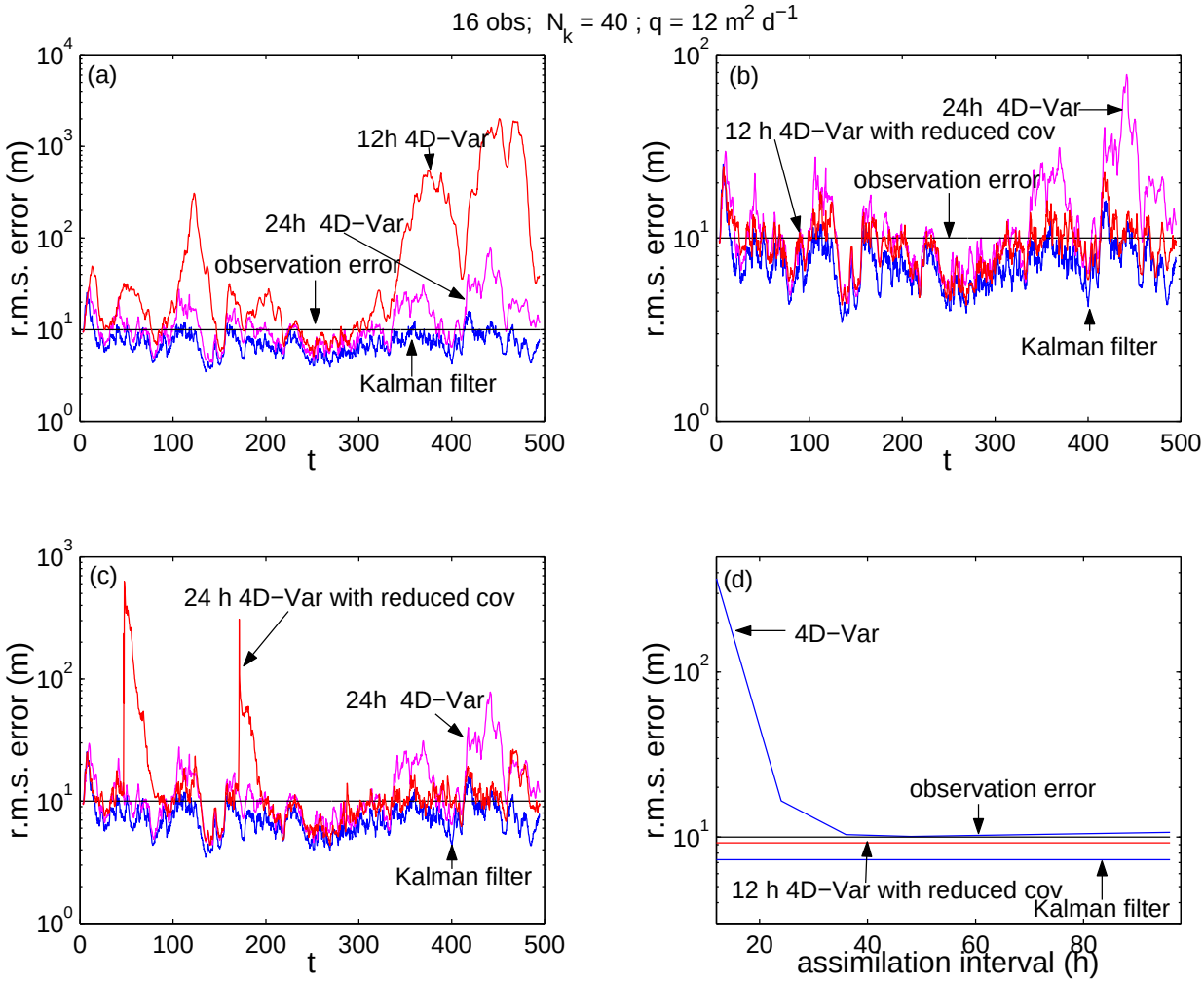

Figure 18: Error in a simulation of the time dependent storm track model with model error. Panel (a): comparison of the errors in a 12 *h and* 24 *h 4D-Var with the error in the full Kalman filter. Panel (b): comparison of the error in a* 24 *h 4D-Var with the error in a* 12 *h 4D-Var in which the isotropic static* **B** *has been preconditioned with the error covariance obtained from a reduced rank Kalman filter with balanced truncation. The reduced rank Kalman filter has been obtained with model error. In the truncated system 40 dof have been retained out of the 400 dof of the system. The isotropic* **B** *introduced to the reduced rank covariance has amplitude equal to the smallest eigenvalue of the reduced rank covariance. Also shown is the error resulting from the Kalman filter. The* 12 *h 4D-Var performance is nearly optimal. Panel (c): comparison of the error in a* 24 *h 4D-Var with the error in a* 24 *h 4D-Var in which the isotropic static* **B** *has been preconditioned with the error covariance obtained from the reduced Kalman filter. The* 24 *h 4D-Var preconditioned with the covariance from the reduced Kalman filter propagates the covariance without model error longer and its performance is worse than that of the corresponding* 12 *h 4D-Var. Panel (d): r.m.s. error in 4D-Var assimilations in the time dependent storm track model with model error as a function of assimilation interval. Also shown is the error obtained with sequential application of a Kalman filter and the error from the* 12 *h 4D-Var which was preconditioned with the reduced rank covariance. 16 observations are assimilated with r.m.s. observational error of* 10 *m. The model error variance coefficient is* $q = 12\ m^2\ d^{-1}$*, so that a model error of* 5 *m accumulates after a day.*

This perspective on assimilation provides insight by allowing generalized stability analysis of the observer system to be performed revealing for instance the distributed error sources that serve to most effectively degrade the analysis (Farrell and Ioannou, 2003).

Analysis of the observer system modelling 4D-Var and the Kalman filter reveals that as the number of observations assimilated increases the analysis error asymptotes to a finite value comparable to observational error and independent of the number of observations unless the forecast error covariance is systematically adjusted to account for the increase of observations. One way this adjustment can be accomplished is by advancing the forecast error covariance in the dynamically relevant reduced order system that supports the growing error structures.

The result from using this accurate forecast covariance is that as the number of observations n increases the associated Kalman filter obtains assimilation error $O(n^{-1/4})$ (with model error present) while the 4D-Var simulation fails to systematically reduce the estimation error. Assuming that redundancy of observation in the restricted subspace of significantly growing error structures has or soon will be available it is important to systematize the error covariance calculation in order to take advantage of these observations.

The gain under the assumption of a perfect model develops far field loading that degrade the assimilation because the model error is in fact non-vanishing. The error covariance obtained by introducing model error into the reduced system suppresses these far field loadings. The error covariance calculated in the reduced system provides a method for introducing model error into 4D-Var thus reducing the deleterious effects of the perfect model assumption and allowing accurate equivalent gains to be realized on short assimilation intervals.

Acknowledgements

This work was supported by NSF ATM-0123389 and by ONR N00014-99-1-0018.

References

Bishop, C. H., B. J. Etherton, S. J. Majumdar, and J. Sharanya, 2001: Adaptive sampling with the ensemble transform Kalman filter. Part I: Theoretical aspects. *Mon. Wea. Rev.*, **129**, 420-436.

Buizza, R, and T. Palmer, 1995: The singular vector structure of the atmospheric general circulation.*J. Atmos. Sci.* **52**, 1434-1456.

Cohn, S. E. and R. Todling, 1966: Approximate Kalman filters for stable and unstable dynamics. *J. Meteor. Soc. Japan*, **75**, 257-288.

Dee, D. P., 1995: On-line estimation of error covariance parameters for atmospheric data assimilation. *Mon. Wea. Rev.*, **123**,1128-1145.

Delsole, T. M. and B. F. Farrell, 1994: Nonlinear Equilibration of Localized Instabilities on a Baroclinic Jet. *J. Atmos. Sci.* , **51**, 22702284.

Dullerud, G.E., and F. Paganini, 2000: *A Course in Robust Control Theory: a Convex Approach*, Springer Verlag, New York, pp 440.

Evensen, G., 1994: Sequential data assimilation with a nonlinear quasi-geostrophic model using Monte-Carlo methods to forecast error statistics. *J. Geophys. Res.*, **99** (C5), 10143-10162.

Farrell, B. F. 1982: Pulse Asymptotics of the Charney Baroclinic Instability Problem. *J. Atmos. Sci.* , **39**, 507517.

Farrell, B. F., and P. J. Ioannou, 1996: Generalized Stability. Part I: Autonomous Operators. *J. Atmos. Sci.* , **53**, 2025-2041.

Farrell, B. F., and P. J. Ioannou, 1999: Perturbation growth and structure in time dependent flows. *J. Atmos.*

Sci. , **56**, 3622-3639.
Farrell, B. F., and P. J. Ioannou, 2001a: Accurate Low Dimensional Approximation of the Linear Dynamics of Fluid Flow. *J. Atmos. Sci.* , **58** 27712789.
Farrell, B. F., P. J. Ioannou, 2001b: State Estimation Using a Reduced-Order Kalman Filter. *J. Atmos. Sci.* , **58**, 36663680.
Farrell, B. F., and P. J. Ioannou, 2005: Optimal excitation of linear dynamical systems by distributed forcing. *J. Atmos. Sci.* , **62**, 460-475.
Fukumori, I., and P. Malanotte-Rizzoli, 1995: An approximate Kalman filter for ocean data assimilation; an example with an idealized Gulf Stream model. *J. Geophys. Res. Oceans*, **100**, 6777-6793.
Gelaro, R., C. Reynolds, and R. M. Errico, 2000: Transient and asymptotic perturbation growth in a simple model. **128**, *Quart. J. Roy. Meteor. Soc.* , 205-228.
Ghil, M., 1997: Advances in sequential estimation for atmospheric and oceanic flows. *J. Meteor. Soc. Japan*, **75**, 289-304.
Ghil, M., and P. Malanotte-Rizzoli, 1991: Data assimilation in meteorology and oceanography. *Adv. in Geophys.*, **33**, 141-266.
Ghil, M., and R. Todling, 1996: Tracking atmospheric instabilities with the Kalman filter. Part II: Two layer results. *Mon. Wea. Rev.*, **124**, 2340-2352.
Glover, K., 1984: An optimal Hankel-norm approximation of linear multivariable systems and their $\mathbf{L}^{\infty}$-error bounds. *Int. J. Control*, **39**, 1115-1193.
Hamill, T.M. 2005. Ensemble-based atmospheric data assimilation. In Palmer, T.N. and Hagedorn, R., editors, Predictability of Weather and Climate. Cambridge University Press.
Houtekamer, P. L., and H. L. Mitchell, 1998: Data assimilation using an ensemble Kalman filter technique, *Mon. Wea. Rev.*, **126**, 796-811.
Ide, K., and M. Ghil, 1997: Extended Kalman filtering for vortex systems. Part I: Methodology and point vortices. *Dyn. Atmos. Oceans*,**27**, 301332.
Ide, K., P. Courtier, M. Ghil, M., and A. C. Lorenc, 1997: Unified notation for data assimilation: operational, sequential, and variational. *J. Meteor. Soc. Japan*, **75**,181-189.
Illyashenko, Yu. S., 1983: On the dimension of attractors of k-contracting systems in infinite-dimensional space. *Vestn. Mosk. Univ. Ser. 1 Mat. Mekh.*, **3**, 52-58.
Kalman, R.E., 1960: A new approach to linear filtering and prediction problems. *J. Basic Eng.*. **82D**, 35-45.
Kalnay, E., Hunt, B., Ott, E., and Szunyogh, I. 2005. Ensemble forecasting and data assimilation: two problems with the same solution? In Palmer, T.N. and Hagedorn, R., editors, Predictability of Weather and Climate. Cambridge University Press.
Kaplan, J. L., and J. A. Yorke, 1979: Preturbulence: a regime observed in a fluid flow model of Lorenz. *Comm. Math. Phys.*, **67**, 93-108.
Lermusiaux, P.F.J., and A. R. Robinson, 1999: Data assimilation via error statistical estimation. Part I: Theory and schemes. *Mon. Wea. Rev.*, **127**, 1385-1407.
Lin, S.J., and R. T. Pierrehumbert, 1993: Is the Midlatitude Zonal Flow Absolutely Unstable?. *J. Atmos. Sci.* , **50**, 505517.
Miller, R. N., M. Ghil, and F. Gauthiez, 1994: Advanced data assimilation in strongly nonlinear dynamical systems.*J. Atmos. Sci.*,**51**, 10371056.
Moore, B. C., 1981: Principal component analysis in linear systems: controllability, observability, and model reduction. *IEEE Trans. on Automatic Control*, **AC-26**, 17-31.
North, G., 1984: Empirical orthogonal functions and normal modes. *J. Atmos. Sci.* , **41**, 879-887.
Palmer, T. N., R. Gelaro, J. Barkmeijer, and R. Buizza, 1998: Singular vectors, metrics, and adaptive observations. *J. Atmos. Sci.* , **55**, 633-653.
Reynolds, C. A., and R. M. Errico, 1999: Convergence of singular vectors towards Lyapunov vectors. *Mon. Wea. Rev.*, **127**, 2309-2323.
Stewart, G. W., and J-G. Sun, 1990: *Matrix Perturbation Theory*, Academic Press, Boston, Massachusetts, pp.

365.
Sznaier, M., A. C. Doherty, M. Barahona, J. C. Doyle, and H. Mabuchi, 2002: A new bound of the $L_2([0,T])$ induced norm and applications to model reduction. *Proc. 2002 American Control Conference*.
Takens, F., 1981: in *Dynamical Systems and Turbulence*, Lecture Notes in Mathematics Vol. 898, edited by D. Rand and L.-L. Young (Springer-Verlag, Berlin,1981), pp. 366-381.
Tippett, M. K., S. E. Cohn, R. Todling, and D. Marchesin, 2000: Low-dimensional representation of error covariance. *Tellus*, **52**,533-553.
Todling, R., and M. Ghil, 1994: Tracking atmospheric instabilities with the Kalman filter. Part I: Methodology and one-layer results. *Mon. Wea. Rev.*, **122**, 183-204.
Zhou, K., and J. C. Doyle, 1998: *Essentials of Robust Control*, Prentice Hall, Upper Saddle River, New Jersey, pp 411.
Van Dooren, P., 2000: Gramian based model reduction of large-scale dynamical systems, in *Numerical Analysis 1999*, Chapman and Hall, CRC Press, London, pp. 231-247.
Verlaan, M. and A. W. Heemink, 1997: Tidal flow forecasting using reduced rank square root filters. *Stochastic Hydrology and Hydraulics*, **11**, 349-368.
Wunsch, C., 1996: *The Ocean Circulation Inverse Problem*, Cambridge University, Cambridge, pp. 442.